

# Research on 2-DOF Antagonistic Bionic Flexible Manipulator\*

Ze Cui, Hongxin Yang, Zenghao Chen and Saishuai Huang

School of Mechatronics Engineering and Automation

Shanghai University, Shanghai, 200444, China

cuize0421@126.com, yhx\_1029@163.com

Danjie Zhu\*\*

Zhejiang Provincial People's Hospital

Hangzhou, Zhejiang Province, 310014, China

zhudj@126.com

**Abstract** - A flexible actuator with variable stiffness was improved in this study, and a 2-DOF flexible manipulator was designed based on the principle of antagonistic motion. To solve the problem of joint redundancy drive, we focused on the position control, stiffness control and position/stiffness decoupling control strategy of antagonistic bionic manipulator. Based on the Lagrange equation, the joint dynamics model was established, and the control model of the joint position and stiffness of the antagonistic bionic joint was proposed. The traditional PID control theory was used to simulate and verify the effectiveness of the above control strategy. Experiments were carried out on the manipulator to verify the rationality of the structure and control model of the manipulator. The experimental results show that the manipulator can achieve more accurate displacement operation under various stiffness conditions according to the control strategy proposed in this paper, and flexible joints can effectively adjust the stiffness and position of the joints when subjected to external loads. The impact can be weakened when collision occurs.

**Index Terms** - Antagonistic joint; Variable stiffness actuator; 2-DOF flexible manipulator

## I. INTRODUCTION

High stiffness drive system is suitable for industrial occasions with high precision requirements, but it has obvious shortcomings in the process of human-computer interaction [1]. The greatest danger in the process of cooperation between robots and humans comes from unpredictable collision. According to the research of Bicchi et al., reducing the contact stiffness in collision can effectively improve the safety of robots [2]. As the core component of a flexible manipulator, variable stiffness actuator can make the manipulator have variable stiffness characteristics, so as to realize power transmission and flexible regulation. The control system of flexible manipulator is used to adjust the stiffness of variable stiffness actuator and to plan the motion path of the manipulator so that the manipulator can achieve both stiffness and position control. But flexible manipulator has the characteristics of nonlinearity, strong coupling and time-varying [3], which makes the design and control of flexible manipulator more complex and difficult.

In the structural design of flexible manipulator, after decades of research by a large number of scholars, lots of

driving prototypes have emerged in different application fields, which have brought convenience to people's lives. Shane A. Migliore et al. proposed a non-linear Variable Stiffness Actuator (VSA) for flexible actuation of robot joints [4]. A driver called Bidirectional Anti-Variable Stiffness (BAVS) can introduce the bidirectional coupling of each motor into the joint to provide greater torque capability [5].

In the control strategy of flexible manipulator, there are two main research routes: one is based on hybrid position/force control, which is mainly used to control the end position of the manipulator and the contact force between the end and the environment [6]; the other is Hogan et al. proposed to adjust the position and contact force of the end-effector through impedance control. Size [7].

We improved a variable stiffness actuator similar to human muscle characteristics, and designed a 2-DOF antagonistic bionic manipulator based on it. Aiming at the problem of redundant joint drive of manipulator, this paper focuses on the position control, stiffness control and position/stiffness decoupling control strategy of antagonistic bionic manipulator. Based on the Lagrange equation, the joint dynamics model was established, and the control model of the position and stiffness of the antagonistic bionic joint was proposed. The antagonistic flexible joint had excellent structural characteristics and position/stiffness decoupling control system could fulfill various requirements more accurately through simulation and experimental research.

## II. DESIGN OF ANTAGONISTIC BIONIC FLEXIBLE JOINT

### A. Design of Nonlinear Variable Stiffness Actuator

Based on the theoretical basis of the nonlinear spring proposed by Shane A. Migliore et al. [8], we improved the structure and obtain a variable stiffness actuator which is more suitable for the antagonistic manipulator, as shown in Fig. 1.

Both springs are always in tension, applying tension to the driver. When the external force acts on the rollers bracket, the relationship between external force and displacement of the bracket along the straight line guideway is a quadratic polynomial,

$$F(\Delta l) = a\Delta l^2 + b\Delta l + c \quad (1)$$

\* This work is supported by Major Science and Technology Projects of Zhejiang Province (2014C3044-2).

\*\* Danjie Zhu is the corresponding author, zhudj@126.com.

Where  $F$  represents the tension of the actuator and  $\Delta l$  indicates the displacement of the bracket along the linear guide. The maximum pulling force of the driver is  $2500N$ , the size is  $120cm \times 125cm$ , and the coefficient was selected as:  $a = 4.804N/cm^2$ ,  $b = 1.574N/cm^2$ ,  $c = 2.571N/cm^2$ .

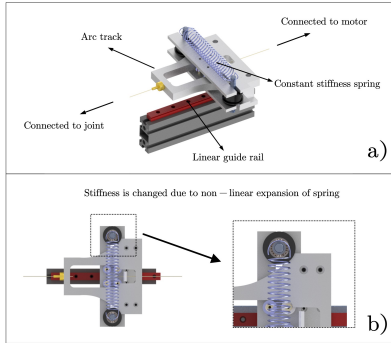


Fig. 1 Nonlinear variable stiffness actuator

### B. Design of 2-DOF Bionic Flexible Manipulator

The rendering diagram of 2-DOF flexible manipulator based on antagonistic mechanism is shown in Fig. 2. It consists of four motors, four non-linear variable stiffness actuators, two joints and two connecting rod arms.

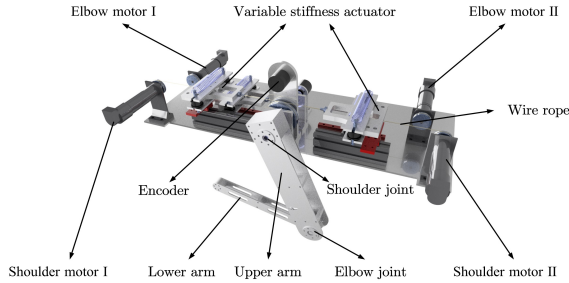


Fig. 2 2-DOF rendering diagram of antagonistic bionic flexible manipulator

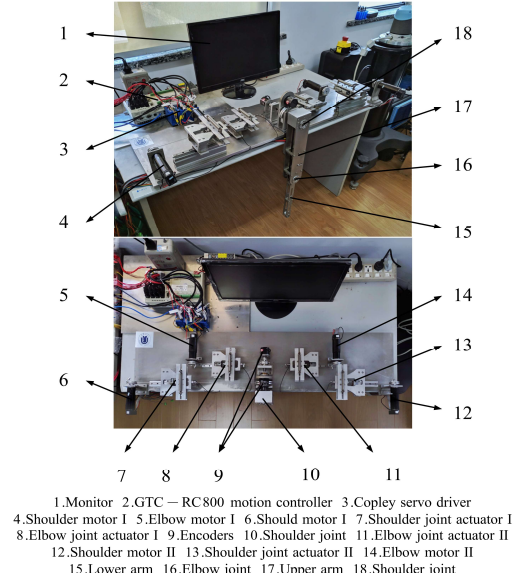


Fig. 3 2-DOF flexible manipulator experimental platform

The flexible manipulator is a motion control system with GTC-RC800 as its control core and DC servo motor as its driving element. The hardware of the system includes PC, Google Technology Motion Controller (GTC-RC800), Copley Servo Driver (ACJ-005-18, USA), Maxon DC Servo Motor (RE-35, Swiss) and Omron Incremental Encoder (E6B2-CWZ1X, China). The overall structure of the system is shown in Fig 3.

### C. Dynamic analysis of shoulder joint

In this paper, the accurate control of the position and stiffness of the shoulder joint was studied. The related parameters are shown in TABLE I.

TABLE I  
RELEVANT PARAMETERS OF SHOULDER JOINT

Physical parameters	Value
Shoulder Joint Shaft Pulley Radius ( $R_s$ )	40 (mm)
Motor shaft pulley radius ( $R_s$ )	20 (mm)
Rotational inertia of shoulder joint ( $I$ )	0.005 (kgm <sup>2</sup> )
Shoulder joint quality ( $m$ )	0.303 (kg)
Length of shoulder joint ( $L$ )	0.3 (mm)
Joint Damping Coefficient ( $D$ )	0.04 (Nms)
Motor moment of inertia ( $J_m$ )	67.9 (gcm <sup>2</sup> )
Motor deceleration ratio ( $n$ )	96:1

The dynamic model of the shoulder joint based on classical Lagrange equation is shown in equation 2. This formula gives the relationship between shoulder joint system and the motor system.

$$\begin{cases} M\ddot{q} + C\dot{q} + D\ddot{q} + G = \tau_E \\ J\ddot{\theta} + D_\theta\theta = \tau_{Ex} + \tau_M \end{cases} \quad (2)$$

Where  $\tau_E$  is the torque of the flexible joint;  $\tau_M$  is the output torque of the motor;  $\tau_{Ex}$  is the external torque of the motor;  $\theta$  and  $\ddot{\theta}$  represent is the position and angular acceleration of the motor;  $q$ ,  $\dot{q}$  and  $\ddot{q}$  indicate the position, the angle and the angular acceleration of the connecting rod;  $J$  is the moment of inertia of the motor;  $M$  is inertia force coefficient.

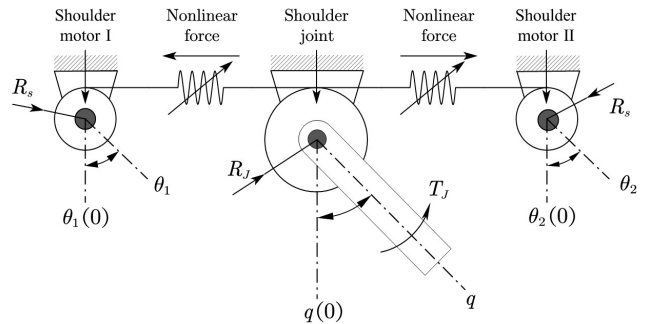


Fig. 4 Antagonistic flexible shoulder joint model

Shoulder joint simplified model is shown in Fig. 4. The two ends of the non-linear variable stiffness actuator are connected with the motor and the joint pulley respectively. The actuator is placed left and right to simulate the two antagonistic

muscles of human joints, forming an antagonistic variable stiffness driving system. The stiffness and position of the joint can be changed in real time by the tension produced by two motors.

$\theta_1$  and  $\theta_2$  are the rotation angles of two motors,  $\theta_1(0)$  and  $\theta_2(0)$  are the initial position of the motor;  $q$  is the rotation angle of the joint,  $q(0)$  is the initial position of the joint;  $R_s$  is the radius of the pulley on the motor shaft,  $R_J$  is the radius of the pulley on the joint shaft. When the shoulder motor I moves from  $\theta_1(0)$  to  $\theta_1$  and the shoulder motor II moves from  $\theta_2(0)$  to  $\theta_2$ , the shoulder joint moves from  $q(0)$  to  $q$ . According to the geometric relationship in Fig. 4, the deformation of two side springs are  $\Delta l_1$  and  $\Delta l_2$  respectively,

$$\Delta l_1 = R_s \theta_1 - R_J q \quad (3)$$

$$\Delta l_2 = R_s \theta_2 + R_J q \quad (4)$$

The forces acting on joints by non-linear springs are  $F_1$  and  $F_2$ ,

$$F_1 = a(R_s \theta_1 - R_J q)^2 + b(R_s \theta_1 - R_J q) + c \quad (5)$$

$$F_2 = a(R_s \theta_2 + R_J q)^2 + b(R_s \theta_2 + R_J q) + c \quad (6)$$

Formulas (3) and (4) are brought into formulas (5) and (6), and the spring elastic potential energy is obtained as follows,

$$\begin{cases} P_{S1}(q_1, \theta_1) = - \sum_{i=1}^n \int_0^{R_s \theta_1 - R_J q_1} (a \Delta l_1^2 + b \Delta l_1 + c) d(\Delta l_1) \\ P_{S2}(q_2, \theta_2) = - \sum_{i=1}^p \int_0^{R_s \theta_2 + R_J q_2} (a \Delta l_2^2 + b \Delta l_2 + c) d(\Delta l_2) \end{cases} \quad (7)$$

The partial derivatives of  $q_1, \theta_1$  and  $\theta_2$  in the upper formula are obtained, obtain the external torque of the joint and the two motors,

$$\tau_E = \tau_E(q, \theta) = R_J(F_1 - F_2) \quad (8)$$

$$\tau_{E1} = \tau_{E1}(q_1, \theta_1) = R_s F_1 \quad (9)$$

$$\tau_{E2} = \tau_{E2}(q_2, \theta_2) = R_s F_2 \quad (10)$$

For single joint system, Coriolis force and centrifugal force coefficient  $C(q, \dot{q}) = 0$ , inertia force coefficient  $M_1 = I + mL^2$ , gravity coefficient  $G_1 = mgLsin\theta$ , motor moment of inertia  $J_1 = J_2 = J_m$ ,  $D_1$  and  $D_2$  are damping coefficients. Taking the shoulder joint as an example, the antagonistic joint dynamics model can be expressed as follows,

$$\begin{cases} M_1 \ddot{q}_1 + D_1 \dot{q}_1 + G_1 = \tau_E \\ J_1 \ddot{\theta}_1 + D_1 \theta_1 = \tau_{E1} + \tau_{M1} \\ J_2 \ddot{\theta}_2 + D_2 \theta_2 = \tau_{E2} + \tau_{M2} \end{cases} \quad (11)$$

Joint stiffness is defined as,

$$K = -\frac{d\tau_E}{dq} = 2aR_s R_J^2 (\theta_1 + \theta_2) + 2bR_J^2 \quad (12)$$

Formula (12) shows that joint stiffness is proportional to the sum of motor rotation angles  $\theta_1$  and  $\theta_2$ . According to the actual test, the sum of motor motion angles of the experimental

platform ranges from 0 to 3 rad, and the maximum stiffness of the joint is about  $1000 Ncm$ .

The basic idea of joint position/stiffness control is that two non-linear variable stiffness actuators can establish the equilibrium position (EP) of the joint. When the joint is in the balanced posture, the resultant force and resultant moment of the joint are zero; if an external force is applied, the joint will be far away from the balanced posture, and when the external force is withdrawn. At the same time, the joint will return to the original balance posture, so the balance posture is a stable state[9]. Applying Feldman's equilibrium position control hypothesis[10], when the shoulder joint is in balance at  $q_{eq}$ ,

$$q_{eq} = \frac{R_s}{2R_J} (\theta_1 - \theta_2) \quad (13)$$

When an external load torque of  $T_{load}$  is applied, the equilibrium position of the joint becomes,

$$q_{eq} = \frac{R_s}{2R_J} (\theta_1 - \theta_2) - \frac{T_{load}}{2R_J^2 [b + aR_s(\theta_1 + \theta_2)]} \quad (14)$$

The values of  $\theta_1$  and  $\theta_2$  can be obtained by formula (12) and (14),

$$(\theta_1, \theta_2) = \frac{K - 2bR_J^2}{4aR_s R_J^2} \pm \frac{R_J}{R_s} \left( q_{eq} + \frac{T_{load}}{S} \right) \quad (15)$$

It can be seen from formula (15) that the rotation angles  $\theta_1$  and  $\theta_2$  of the motor can simultaneously control the balance position and stiffness of the joint, and no additional motor is needed. Therefore, the stiffness and position of the joint can be adjusted in real time in the course of movement.

### III. CONTROL STRATEGY OF ANTAGONISTIC BIONIC FLEXIBLE JOINT

#### A. Flexible Joint Control Strategy

In closed-loop control of joint position, joint position  $q$  is determined by motor rotation angle  $\theta_1$  and  $\theta_2$ , and joint stiffness  $K$  is also determined by the two angles, so there is a coupling relationship between  $q$  and  $K$ , which belongs to redundant drive mode. By using this driving method, the manipulator can not only satisfy the displacement operation, but also make the system achieve the required stiffness. In order to achieve various types of force/position constraints, the position and stiffness control of the system can be decomposed into the control of the motion positions of two motors.

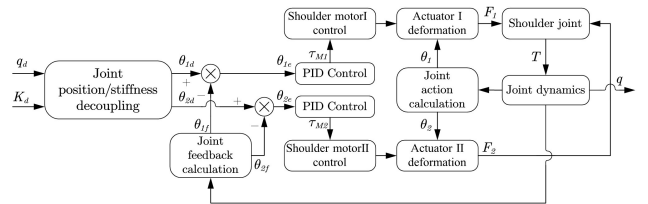


Fig. 5 Flexible joint control block diagram

For antagonistic bionic joints, the control strategies can be subdivided into position control, stiffness control and position/stiffness decoupling control. The control block

diagram of this study is shown in Fig. 5. The expected stiffness and position of the joint are taken as the input of the system. When the two variables change, the rotation of the servo motor is adjusted by PID control [11], so that the joint has certain dynamic characteristics while ensuring the position accuracy.

### B. Motion simulation of flexible joint

The system simulation experiment is carried out under the environment of MATLAB/Simulink, and the whole simulation process is solved by Ode23s integrator. Joint Dynamics Equation Reference Formula (2), Target Position Reference Formula (15) for two motors.

#### 1) Position control simulation

The position control of the joint is to take the desired trajectory of the joint as the input of the system and compare the actual trajectory of the joint under different stiffness conditions. The desired trajectory is square and sinusoidal signals with amplitude of 1 rad and the stiffness was set to 100Ncm/rad, 400Ncm/rad, 700Ncm/rad, 1000Ncm/rad.

The simulation results of tracking the two waveforms are shown in Fig. 6 (a) and (c). The Fig. 6 (b) and 6 (d) are error curves. On the whole, the system had better response characteristics. When the stiffness of the system is large, the system can quickly reach a stable state and achieve more accurate control. When the stiffness of the system is low, due to the inertia of the manipulator, the system has a certain degree of overshoot, and there will be a lag phenomenon in the actual position curve, the error is bigger than the former.

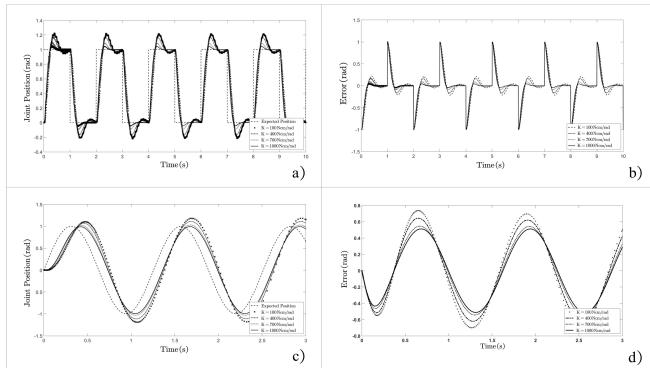


Fig. 6 Simulated curves of square and sinusoidal wave tracking

#### 2) Stiffness control simulation

Stiffness control of joint is to take the expected stiffness of joint as the input of the system and observe the actual stiffness in the process of periodic motion. The expected stiffness were set to 100Ncm/rad, 400Ncm/rad, 700Ncm/rad and 1000Ncm/rad, and then additional loads were applied to the system to test the dynamic performance of the system. The desired position of the joint was set as a sinusoidal curve, and the actual position of the joint and the corresponding stiffness changes in the simulation experiment were collected. The joint position curve is shown in Fig. 7 (a) and the real-time stiffness of the joint is shown in Fig. 7 (b).

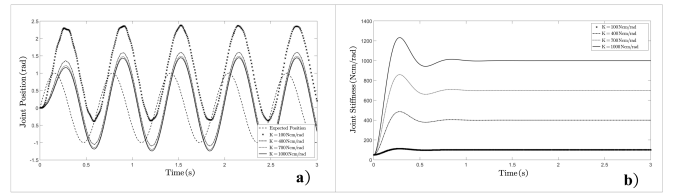


Fig. 7 Change curve of joint position and stiffness

There is overshooting in the system in order to achieve different expected stiffness under the interference of external moment, and the initial oscillation of the system is obvious. With the adjustment of spring contraction, the system error can decrease, and finally reach stability, and the change of joint stiffness will also tend to be stable. For systems with larger expected stiffness, the stiffness adjustment and the amplitude of the position following are smaller, and the system can achieve stability quickly, and vice versa.

#### 3) Position/stiffness decoupling control

The position/stiffness control of the joint takes the desired position  $\theta_d$  and the expected stiffness  $K_d$  of the joint as the input of the system. After decoupling operation of the control system, the two input variables are mapped to the real-time positions  $\theta_1$  and  $\theta_2$  of the two motors. During the experiment, the actual position and stiffness of the joint were recorded in periodic and non-periodic motion.

The desired position  $\theta_d$  of the joint was set as sine signal and step signal, and the desired stiffness  $K_d$  of the joint was set as random signal (square wave of amplitude  $400 \pm 300$  Ncm/rad) and sine wave signal, as shown in Fig. 8 (a). The real-time position and stiffness curves of the joint are shown in Fig. 8 (b) and Fig. 8 (c).

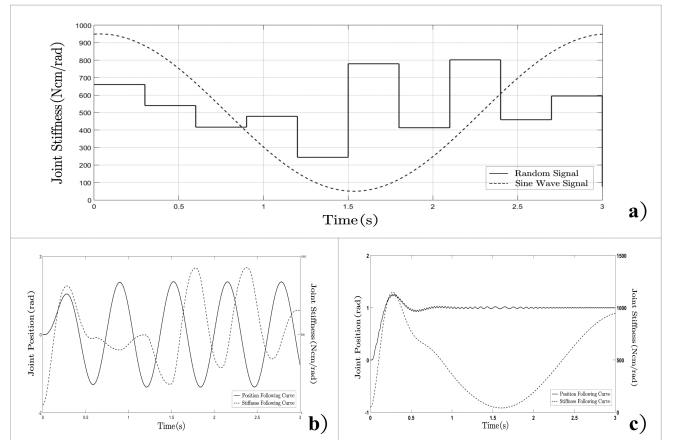


Fig. 8 Following curve of joint position and stiffness

From the simulation results, it can be seen that the real-time stiffness in Fig. 8 (b) is always changing in 3 seconds, and the stiffness control fluctuates, but the overall stiffness change trend is consistent with the expected value. In Fig. 8 (c), there are a few lags and overshoots in the real-time position adjustment of the joint, but they can be corrected in time.

#### IV. EXPERIMENTAL VERIFICATION

In Chapter III, the control strategy of joint position and stiffness has been analyzed in a simulation environment. In this chapter, a number of experiments will be carried out to test the performance of flexible manipulator and control system in real scene.

##### A. Stiffness and position control of shoulder joint

Stiffness adjustment ability of shoulder joint and the accuracy of in-place operation under different stiffness conditions were tested in this experiment. The experimental process of stiffness control is as follows: the stiffness of the joint was increased slowly from  $0\text{Ncm}/\text{rad}$  to  $800\text{Ncm}/\text{rad}$ , and then slowly reduced to  $0\text{Ncm}/\text{rad}$  after a period of time. Then the expected stiffness is changed every 5 seconds, from  $0\text{Ncm}/\text{rad}$  to  $800\text{Ncm}/\text{rad}$ , and input is divided into 8 stages. In this process, the input expected stiffness and the tension information feedback from the left and right joint tension sensors are compared.

The experimental results are shown in Fig. 9. When the expected stiffness of the system is changed, the system can respond quickly. The spring tension value will change immediately, and the actual stiffness increases accordingly.

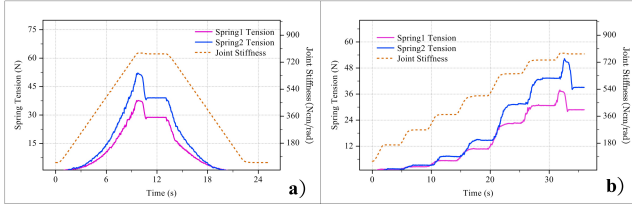


Fig. 9 Experimental results of joint variable stiffness

The experimental process of position control is as follows: To increase joint stiffness gradually to the target value in the natural state. When the joint stiffness tends to stabilize, input the desired joint position  $\theta_d$ , and obtain the actual joint position  $q$  through the encoder. By comparing the difference between  $\theta_d$  and  $q$ , we can know the position control accuracy of the manipulator under different stiffness conditions. The experimental results are shown in Fig. 10 (a) and the joint angle error curve are shown in Fig. 10 (b).

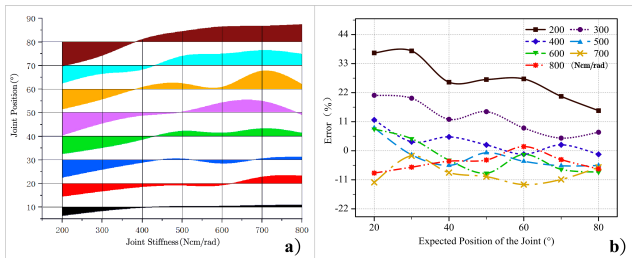


Fig. 10 Experimental results and error curves of position control

From the experimental results, it can be seen that the error of joint displacement operation under low stiffness state ( $\leq 300\text{Ncm}/\text{rad}$ ) is large, and in medium and high stiffness state ( $\geq 300\text{Ncm}/\text{rad}$ ) better control accuracy can be

guaranteed, and the error can be controlled within 10% as a whole.

##### B. Dynamic load experiment

Impulse load was applied at the end of the arm to test the adjusting ability of shoulder joint under different stiffness conditions. Firstly, different stiffness values of shoulder joint were preset, and the position of shoulder joint was adjusted to 80 degrees. When the joint reaches the preset stiffness and position, a certain weight is released at the end of the joint instantaneously. The experimental processes are shown in Fig. 11.

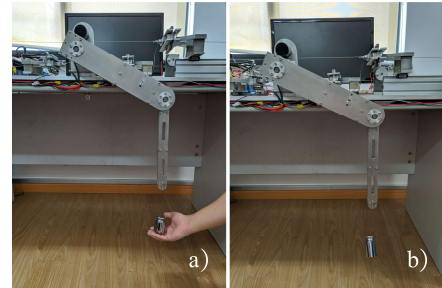


Fig. 11 Dynamic load experiment process

The weights of 0.3kg, 0.5kg and 0.7kg are mounted at the end of the joint. Referred to the length and rotation angle of the manipulator, the impact loads on the end of the joint can be calculated as  $88.65\text{Ncm}$ ,  $147.75\text{Ncm}$  and  $206.85\text{Ncm}$ . The self-adjustment of shoulder joint position under different impact loads is recorded. The experimental results are shown in Fig. 12. The presupposed stiffness of Fig. 12 (a), (b) and (c) are  $200\text{Ncm}/\text{rad}$ ,  $400\text{Ncm}/\text{rad}$ ,  $600\text{Ncm}/\text{rad}$  respectively.

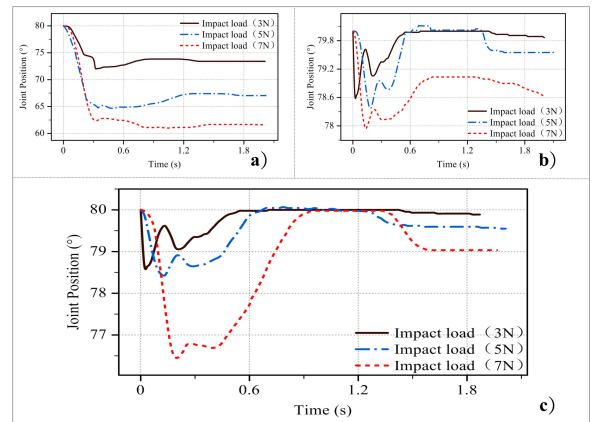


Fig. 12 Position adjustment of the shoulder joint after impact

When the joint is subjected to the same impact load, the high stiffness system has shorter stable time, smaller joint deflection and oscillation than the low stiffness system. Although high stiffness can bring higher positioning accuracy, the impact on the contact is also the greatest. When the flexible joint is impacted, the flexible element of the joint can absorb part of the energy, and absorbed impact energy is inversely proportional to the stiffness of the joint, which can effectively reduce the damage to the contact material.

### C. Collision experiment

In order to detect the force acting on the contacts when the flexible manipulator suddenly collides under different stiffness conditions, the force magnitude can directly reflect the influence of joint stiffness on the manipulator and the external scene. The platform of the collision experiment is shown in Fig. 13. The six-dimensional force sensor below is ATI FT12760. Sampling frequency is set to 7000Hz.

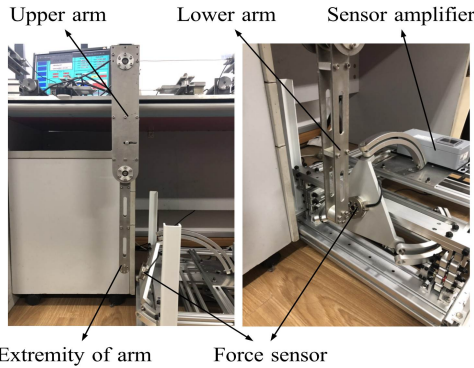


Fig. 13 Collision experiment scene

The experiment process is as follows: First, the manipulator was moved to the designated position, then adjusted the shoulder joint stiffness to the preset values ( $400\text{Ncm/rad}$  and  $800\text{Ncm/rad}$ ). To control the elbow joint so that the lower arm was always perpendicular to the ground, then made the end of the manipulator move downward rapidly until it collided with the force sensor below, and finally recorded the value produced by the force sensor. According to the resultant force relationship, the end contact force  $F$  was calculated by the force recorded by the sensor in three directions of  $F_x$ ,  $F_y$  and  $F_z$ . The experimental results are shown in Fig.14, (a) and (b) represent different initial positions of the manipulator, which are 30 degrees and 60 degrees.

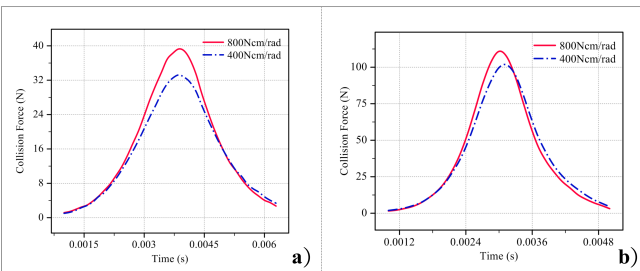


Fig. 14 Change curve of end impact force

The experimental results show that the higher the initial position of the joint, the greater the contact force produced when the end of the joint collides. Because the contact time between the end of the joint and the sensor is in short time (about 0.006s), the instantaneous acceleration is large, which has a high risk of damage to the manipulator and the contacts. But it can also be seen from Fig. 14 that the joints in the low stiffness state can effectively reduce the impact force and reduce the damage when collisions occur.

### V. CONCLUSION

Based on the principle of variable stiffness flexible drive, a 2-DOF antagonistic variable stiffness flexible manipulator and relevant control strategy were established, and the effectiveness of shoulder joint stiffness control, position control and position/stiffness decoupling control were verified through simulation and experiment. The following progress has been made in this study:

- 1) Based on Lagrange equation and the theory of antagonistic variable stiffness, the dynamic model of a flexible manipulator was established, and the position/stiffness decoupling control model of 2-DOF antagonistic bionic flexible manipulator was further established.
- 2) The simulation model of the shoulder joint of the manipulator was built by using MATLAB/Simulink, which proves that the control strategy is feasible above.
- 3) Complete the design of 2-DOF antagonistic bionic flexible manipulator and its control system. Experiments showed that the platform can satisfy all kinds of stiffness and position requirements better and enhance the safety of human-machine interaction.

Although this paper has achieved some research results, it still needs to be further studied in the following aspects:

- 1) In this study, feed-forward method was used to correct the deviation of damping, which results in large errors in the actual system.
- 2) At present, only the shoulder joint of the manipulator was studied in this paper. Next, the control algorithm of the two joints of the flexible arm will be studied deeply.

### REFERENCES

- [1] G.-l. Xiong, Z.-w. Xie, J.-b. Huang, H. Liu, Z.-n. Jiang, and K. Sun, "Dynamic surface control-backstepping based impedance control for 5-DOF flexible joint robots," *Journal of Central South University of Technology*, vol. 17, no. 4, 2010.
- [2] B. Vanderborght, A. Albu-Schaeffer, A. Bicchi, E. Burdet, D. G. Caldwell, R. Carloni, M. Catalano, O. Eiberger, W. Friedl, and G. Ganesh, "Variable impedance actuators: A review," *Robotics & Autonomous Systems*, vol. 61, no. 12, pp. 1601-1614, 2013.
- [3] T. K. Chang, A. Spowage, and K. Y. Chan, "Review of Control and Sensor System of Flexible Manipulator," *Journal of Intelligent & Robotic Systems*, vol. 77, no. 1, pp. 187-213, 2015.
- [4] T. Menard, G. Grioli, and A. Bicchi, "A Stiffness Estimator for Agonistic–Antagonistic Variable-Stiffness-Actuator Devices," *IEEE Transactions on Robotics*, vol. 30, no. 5, pp. 1269-1278, 2014.
- [5] F. Petit, W. Friedl, H. Höpner, and M. Grebenstein, "Analysis and Synthesis of the Bidirectional Antagonistic Variable Stiffness Mechanism," *Mechatronics IEEE/ASME Transactions on*, vol. 20, no. 2, pp. 684-695, 2015.
- [6] B. Siciliano, and L. Villani, "Robot Force Control," *Springer Berlin*, 2013.
- [7] N. Hogan, "Impedance Control: An Approach to Manipulation."
- [8] S. A. Migliore, E. A. Brown, and S. P. Deweerth, "Biologically Inspired Joint Stiffness Control."
- [9] R. V. Ham, T. G. Sugar, B. Vanderborght, K. W. Hollander, and D. Lefebvre, "Compliant actuator designs," *IEEE Robotics & Automation Magazine*, vol. 16, no. 3, pp. 81-94, 2009.
- [10] A. G. Fel'Dman, "[On the functional tuning of the nervous system in movement control or preservation of stationary pose. II. Adjustable parameters in muscles]," *Biofizika*, vol. 11, no. 3, pp. 498, 1966.
- [11] A. Datta, M. T. Ho, and S. P. Bhattacharyya, *Structure and Synthesis of PID Controllers*, 2000.